Geotechnical Testing Journal

doi:10.1520/GTJ20230353 / Vol. 47 / No. 3 / 2024 / available online at www.astm.org

Jia-ren Yu[1] and Chao Zhou[1,2]

A New Multiphase Apparatus for Testing Soil Permeated with Three Immiscible Fluids

Reference

J. Yu and C. Zhou, "A New Multiphase Apparatus for Testing Soil Permeated with Three Immiscible Fluids," *Geotechnical Testing Journal* 47, no. 3 (May/June 2024): 653–669. https://doi.org/10.1520/GTJ20230353

ABSTRACT

Oil-contaminated unsaturated soil is a complex multiphase material. In this study, a new triaxial apparatus was developed to independently control/measure its air, oil, and water pressures. Therefore, the suctions associated with air–water, air–oil, and oil–water interfaces can be determined. The apparatus utilizes the hanging column and axis-translation techniques to control suctions in 0~5 kPa and 5~600 kPa. It is suitable for investigating water/oil retention, isotropic compression, and triaxial shear behavior of oil-contaminated soil. Using this new apparatus, five tests were conducted to analyze the saturation–pressure (*S*–*P*) relationship of sand and sandy silt at various oil and water contents and to evaluate the validity of the axis-translation technique for soil permeated with three nonimmersible fluids. Results showed that the artificial increase of air pressure in the axis-translation technique does not obviously alter the air–water and air–oil suctions at constant oil and water contents. A popular suction–saturation model, which was proposed based on test results of clean sands, showed a good prediction of the air–oil suction. However, the oil–water suction results of sandy silt do not align with the model prediction, suggesting that the model may need to be revised for soils with some silt and clay particles.

Keywords

laboratory tests, partial saturation, oil contamination, suction, axis-translation technique

Manuscript received March 2, 2023; accepted for publication November 1, 2023; published online January 29, 2024. Issue published May 1, 2024.

[1] Department of Civil and Environmental Engineering, The Hong Kong Polytechnic University, 181 Chatham Rd. S., Hung Hom 999077, Hong Kong, https://orcid.org/0000-0003-4419-484X (J.Y.)

[2] Shenzhen Research Institute, The Hong Kong Polytechnic University, 18 Yuexing 1st Rd., Nanshan District, Shenzhen 518057, China (Corresponding author), e-mail: c.zhou@polyu.edu.hk, https://orcid.org/0000-0002-9443-6707

Introduction

Soil contamination by oil and other hydrocarbons is a worldwide problem due to storage tank leakages, pipeline breaks, transportation accidents, etc. Apart from posing long-term risks to the environment and human health, oil contamination can adversely affect

FIG. 1 Schematic and phase diagram of oil-contaminated unsaturated soil.

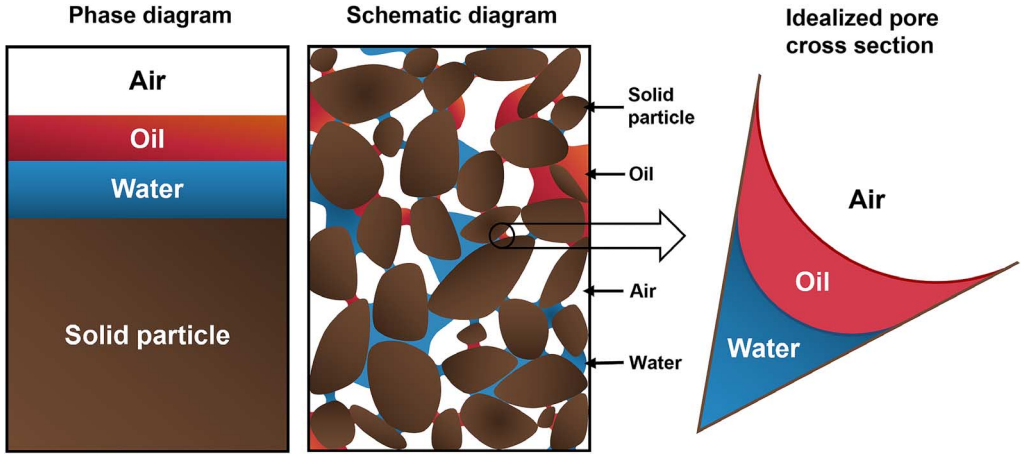

the engineering characteristics, such as reducing the uplift capacity of concrete piles (Nasr 2013), decreasing the bearing capacity of rigid strip footings, and causing additional foundation settlement (Nasr 2009). Oil-contaminated sites need to be managed effectively for various purposes, including assessing the movement of oil in the soil (Essaid et al. 2011), understanding the affected zone and distribution in the ground (Cassiani et al. 2014; Wang et al. 2020), evaluating the impact of oil leakage on nearby earthen structures and slopes (Little 2023), and designing a remediation strategy (Ossai et al. 2020). For these purposes, the hydro-mechanical behavior of oil-contaminated soil at saturated and unsaturated conditions should be understood (Lenhard, Rayner, and Davis 2017; Lenhard et al. 2018; Boumaiza et al. 2022), such as the oil and water retention ability, compressibility, and shear behavior. On the other hand, the presence of oil makes soil testing more challenging, especially under unsaturated conditions. An oil-contaminated unsaturated soil is a four-phase material (see **fig. 1**) with strong interactions between different phases. Independent control of stress, pore water, and oil and air pressures is required in an ideal testing apparatus for this material.

Some apparatuses have been developed by previous researchers (Lenhard and Parker 1988; Busby, Lenhard, and Rolston 1995; Cui, Delage, and Alzoghbi 2003; Abidoye and Das 2014) to test oil-contaminated soil, as summarized in **Table 1**. Water and oil retention behavior, also known as the saturation–pressure (S–P) relationship, is the focus of these studies because it is a fundamental parameter (Tomlinson et al. 2014; Sale, Hopkins, and Kirkman 2018). The first apparatus was developed by Lenhard and Parker (1988) to directly measure the S–P relationships of three fluid phases (i.e., water, oil, and air). Hydrophilic and hydrophobic porous ceramics were used to control the oil and water pressures separately in the pressure range of −40~0 kPa on a sand column. The air was connected to the atmosphere, and the pressure was assumed to be 0 kPa. The two-liquid-phase (oil–water) S–P relationship was verified by the data from this apparatus. It was also employed to predict the three-fluid-phase (air–oil–water) system S–P relationship of sand (Lenhard and Parker 1988) and validated a hysteretic S–P model for oil-contaminated sand by Lenhard (1992). This method was applied to different soil types and studied the S–P relation of sand and loam by Busby, Lenhard, and Rolston (1995). However, the pore air pressure could not be controlled by this method, limiting the measurement and control of air–water and air–oil suctions to 100 kPa. In addition, these apparatuses were unavailable to apply stress control on the soil sample. The axis-translation technique was adopted by Cui, Delage, and Alzoghbi (2003) to control suctions in a wide range. An air pressure controller was added to modify Lenhard's design. Different air pressures could be applied to the specimen, increasing the air–oil suction range to hundreds of kPa. The shape of the porous ceramics (from rings to plates) was also changed for one-dimensional stress control, allowing for the successful measurement of oil

TABLE 1
Technical features of the previous apparatus and the newly developed one

Reference	Stress Control	Deformation Measurement	Fluid Pressure Control	Pressure Control	Available Suction Range	Suitable Soil Type	Saturation Measurement
Lenhard and Parker (1988)	Not controllable	No	Oil, water	$u_a = 0$ kPa $u_w = -40 \sim 0$ kPa $u_o = -20 \sim 0$ kPa	0∼100 kPa	Sand	Fluid volume change monitoring
Busby, Lenhard, and Rolston (1995)	Not controllable	No	Oil, water	$u_a = 0$ kPa $u_w = -40 \sim 0$ kPa $u_o = -10 \sim 0$ kPa	0∼100 kPa	Sand, loam	Fluid volume change monitoring
Cui, Delage, and Alzoghbi (2003)	One-dimensional	No	Air, oil, water	Axis-translation $u_a = 0 \sim 300$ kPa $u_w = 0 \sim 300$ kPa $u_o = 0$ kPa	0∼500 kPa or higher	Sand, silt, clay	Fluid volume change monitoring
Abidoye and Das (2014)	Not controllable	No	Air, oil, water	Hanging column $u_a = 0$ kPa $u_w = -20 \sim 0$ kPa $u_o = -20 \sim 0$ kPa	0∼30 kPa	Sand	TDR transducer
Newly developed in this study	Triaxial	Yes	Air, oil, water	Axis-translation $u_a = 0 \sim 600$ kPa $u_w = -40 \sim 600$ kPa $u_o = -40 \sim 600$ kPa	0∼600 kPa or higher (depends on the ceramic plate)	Sand, silt, clay	Fluid volume change monitoring

retention curves in compacted silt with different densities and permeabilities. Only the retention behavior of two-fluid-phase (i.e., air–water particle and air–oil particle) systems was tested by Cui, Delage, and Alzoghbi (2003), and the validity of using the axis-translation technique in a three-fluid-phase (air–oil–water) system has yet to be verified through experimental data. Fluid volume change monitoring was used in all three of the aforementioned apparatuses to measure the variation of liquid saturation. This saturation measurement method was modified by Abidoye and Das (2014) by incorporating a time domain reflectometry (TDR) probe to measure water saturation in the retention test. Despite these developments, no apparatus has been applied to independently control air, oil, and water pressures in a wide range. Contact probems between the mold and sample along a drying path due to soil shrinkage would be encountered by the existing apparatuses. Another limitation is that soil volume change could not be measured during the testing. In addition, the confining pressure and vertical stress on the sample could not be applied. These limitations challenge researchers seeking to better understand oil-contaminated soil's complex hydro-mechanical behavior.

This paper presents the development of a new triaxial apparatus that can independently control stress and three fluid pressures in oil-contaminated unsaturated soil. A series of tests were conducted using this apparatus to evaluate the validity of the axis-translation technique (Ng, Zhou, and Leung 2015), which has been verified for three-phase but not four-phase porous material in the literature. Moreover, the results of these tests were used to review an existing and widely used *S*–*P* model (Parker, Lenhard, and Kuppusamy 1987), which has been verified based on test results of oil-contaminated clean sands but not other soils.

Development of the New Apparatus

A triaxial testing apparatus has been modified for testing the hydro-mechanical behavior of multiphase oil-contaminated unsaturated soil. Oil and water retention, isotropic compression, and triaxial shear tests can be carried out on oil-contaminated soil under different stress conditions using this apparatus. **Figure 2** shows the schematic diagram of the new apparatus. It consists of a triaxial frame, cell, flushing system, pressure regulators, pressure

FIG. 2 Three-phase pressure- and saturation-controlled triaxial apparatus: (*A*) schematic diagram (dimensions are indicated in millimeters); (*B*) prototype, control system, and the installed soil specimen.

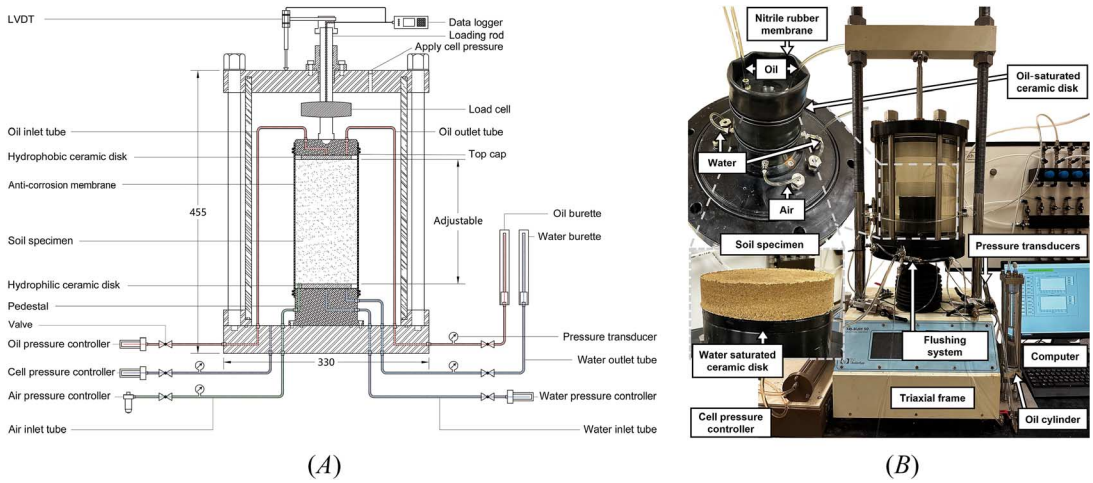

transducers, data logger, and computer. The components within the cell are drawn to scale, whereas the remaining components outside are not drawn to the same scale for clarity.

The pressures of three phases (water, oil, and air) of soil specimens can be independently controlled and measured by this apparatus. The soil specimen is in contact with two ceramic disks, one hydrophobic and one hydrophilic. The lower porous ceramic disk is naturally hydrophilic (Busby, Lenhard, and Rolston 1995) and is used to measure and control pore water pressure. It is in contact with the soil sample through the filter paper and connected to a water pressure transducer, a flushing system, and a pressure/volume controller (VJ Tech) that allows for the measurement of water volume change in the channel and the control of water pressure. The diffusion-induced air bubbles could be removed by a flushing system in the liquid channel. Without flushing for a period, the measured matric suction value is unreliable if diffused air is not removed (Vanapalli, Nictotera, and Sharma 2009).

The porous ceramic disk on the top cap has been chemically treated to be hydrophobic, allowing for the accurate measurement of oil pressure in a mixed multiphase flow using oil-filled channels and transducers on the treated ceramic disk. This treatment process, described in Cui, Delage, and Alzoghbi (2003), involves cleaning the ceramic disk with sodium hydroxide, air-drying it, immersing it in a Glassclad 18 solution for 20 minutes, rinsing it with water, and then curing it in an oven at 100°C for 90 minutes. The resulting hydrophobic ceramic disk is waterproof and maintains its properties over an extended period. This ceramic disk is in contact with the soil sample through the filter paper and connected to an oil pressure transducer, a flushing system, and an oil cylinder that allows for the measurement of oil volume change and the control of oil pressure using an air pressure regulator. By saturating the hydrophobic disk with oil and the hydrophilic disk with water, the pressure controllers in each channel can separately regulate and measure the oil and water pressures. The air channel is directly connected to the soil sample and controlled by an air pressure regulator. The cell water pressure is regulated using another pressure/volume controller (VJ Tech).

According to the accuracy requirement for different soil types in this modified apparatus, hanging column and axis-translation techniques are utilized to control the suction levels, which has been validated by some pioneering work (e.g., Ahmadinezhad, Jafarzadeh, and Sadeghi 2019). When using the hanging column, the air channel is connected to the atmosphere ($u_a = 0$ kPa), and the water/oil pressures were controlled by altitude difference at −40~0 kPa. This pressure-controlling method is appropriate for sand with a low suction range and high accuracy requirement. When using the axis-translation technique, the air pressure can be adjusted

to increase so the range of available suction can be increased up to 600 kPa, depending on the air-entry value of the ceramic disks (hydrophilic disk with water: 300 kPa; hydrophobic disk with oil: 136 kPa). This expands the suitability of the apparatus to a wider range of soil types, including silt and clay.

A customized nitrile rubber membrane is adopted to substitute the conventional latex membrane wrapping the soil sample to avoid oil corrosion to the membrane during long-term testing. A linear variable differential transformer (LVDT) is used to measure the sample volume change during the testing. This apparatus provides a valuable means of studying the properties and behavior of oil-contaminated unsaturated soil, allowing for an accurate evaluation of three-fluid-phase pressure conditions, stress conditions, and soil volume changes within the specimen.

Test Program and Procedures

Some tests were carried out using the new apparatus. The first objective is to evaluate the validity of the axis-translation technique for soil permeated with three nonimmersible fluids (i.e., a solid–air–oil–water system in this study). Note that the axis-translation technique was previously used to test soils with two types of fluids (air–water or air–oil) (Cui, Delage, and Alzoghbi 2003). Its validity in the complex three-fluid-phase systems involving air–water, oil–water, and air–oil interfaces has yet to be evaluated through experimental data. The test program is shown in **Table 2**, consisting of one test on clean sand and four specimens on sandy silt. On the one hand, the test No. 1 on clean sand applies a moisture condition of $S_W = 0.40$ and $S_O = 0.15$. The S_W is the water volume divided by the total pore volume. Similarly, the S_O is the ratio of oil volume and total pore volume. Each specimen was subjected to 10-kPa air pressure and 110-kPa cell pressure at the given S_O and S_W. After reaching an equilibrium state, the air and cell pressures would simultaneously increase stepwise (by 10 kPa at each step) at constant oil and water conditions. The final air and cell pressures were 50 kPa and 150 kPa, respectively, and the net stress (cell pressure minus air pressure) was kept constant during the test. On the other hand, the tests on the sandy silt considered different degrees of water saturation S_W and degrees of oil saturation S_O (No. 2: $S_W = 0.55$, $S_O = 0.15$, $S_A = 0.30$; No. 3: $S_W = 0.55$, $S_O = 0.20$, $S_A = 0.25$; No. 4: $S_W = 0.55$, $S_O = 0.30$, $S_A = 0.15$; No. 5: $S_W = 0.70$, $S_O = 0.15$, $S_A = 0.15$). The test procedures were similar to those for clean sand except for one difference. The air and cell pressures were simultaneously increased by a larger value (i.e., 100 kPa) at each step because the air–water suctions in sandy silt would be over 100 kPa. Therefore, the initial and final air pressures were 200 kPa and 600 kPa, and the initial and final cell pressures were 300 and 700 kPa, respectively. The valves of the oil and water channel were closed with the measurement of oil and water pressures.

The second objective is investigating the *S*–*P* relationships at various oil and water saturation conditions. The test program includes the suctions measurement in the mentioned five specimens, as summarized in **Table 2**. The test results of the *S*–*P* relationship could be used to evaluate the theoretical model proposed by Parker, Lenhard, and Kuppusamy (1987), which has been verified by using the results of clean sand but not other soils.

TEST MATERIALS AND SPECIMEN PREPARATION

As explained in the previous section, a clean sand (Fujian standard sand) (Ye, Lu, and Ye 2015) was used for the first objective. The tested clean sand was categorized as poorly graded sand (ASTM D2487-11, *Standard Practice for Classification of Soils for Engineering Purposes (Unified Soil Classification System)* (Superseded)), and the median particle size was 0.375 mm. The minimum and maximum dry density are 1.49 g/cm^3 and 1.76 g/cm^3, respectively ($e_{max} = 0.797$ and $e_{min} = 0.526$). A completely decomposed granitic (CDG) soil, categorized as silt (ASTM D2487-11), was tested for both objectives. The liquid and plastic limits are 31.6 % and 21.2 %, respectively. The particle size distribution of sandy silt was measured following (ASTM D7928-17, *Standard Test Method for Particle Size Distribution (Gradation) of Fine-Grained Soils Using the Sedimentation (Hydrometer Analysis)*), and the results are shown in **figure 3*A***. In addition, the soil–water retention curve of the oil-free CDG soil was measured using a similar apparatus, and the results are plotted in **figure 3*B***. These experimental data points were fit using the van Genuchten (VG) model (van Genuchten 1980) and can serve as a benchmark for

TABLE 2

Test program and results in each stage

Number	Soil Type	Fluid Saturations				Void Ratio		Stage	Applied Pressures, kPa		Pressures after Equilibrium, kPa			Suctions after Equilibrium, kPa			Equilibrium Time, h	
		Water	Oil	Total	Air	Before Test	During Test		Cell	Air	Air	Oil	Water	Air–Oil	Oil–Water	Air–Water	Oil	Water
1	Clean sand	0.40	0.15	0.55	0.45	0.35	0.35	1.1	110	10	10.4	9.9	8.9	0.5	1.0	1.5	0.9	1.1
								1.2	120	20	20.2	19.6	18.6	0.6	1.0	1.6	0.8	1.0
								1.3	130	30	30.2	29.6	28.6	0.6	0.9	1.5	1.0	0.9
								1.4	140	40	40.1	39.6	38.6	0.5	1.0	1.5	1.0	0.9
								1.5	150	50	50.3	49.8	48.9	0.6	0.9	1.5	1.1	0.9
2	Sandy silt	0.55	0.15	0.70	0.30	0.49	0.48	2.1	300	200	199.7	191.5	70.1	8.2	120.0	129.6	12	20
								2.2	400	300	300.2	290.8	170.8	9.4	118.3	129.4	6	17
								2.3	500	400	402.6	391.7	272.7	10.9	118.8	129.9	6	12
								2.4	600	500	499.4	487.0	366.1	12.4	117.8	133.3	11	12
								2.5	700	600	599.8	586.5	462.7	13.3	120.3	137.1	7	10
3	Sandy silt	0.55	0.20	0.75	0.25	0.49	0.48	3.1	300	200	200.2	193.7	142.9	6.5	49.5	57.3	9	7
								3.2	400	300	299.9	292.2	242.5	7.7	45.5	57.4	8	7
								3.3	500	400	400.2	393.4	344.2	6.8	46.8	56.0	8	7
								3.4	600	500	500.9	492.9	441.8	8.0	50.7	59.1	10	8
								3.5	700	600	599.2	591.8	540.3	7.4	48.2	58.9	10	7
4	Sandy silt	0.55	0.30	0.85	0.15	0.49	0.48	4.1	300	200	199.4	197.3	162.2	2.1	31.0	37.2	13	4
								4.2	400	300	300.8	297.9	261.9	2.9	33.4	38.9	10	4
								4.3	500	400	400.4	397.0	369.4	3.4	28.4	31.0	10	6
								4.4	600	500	501.0	497.5	471.0	3.5	26.7	30.0	9	6
								4.5	700	600	600.2	596.5	570.0	3.7	26.2	30.2	7	6
5	Sandy silt	0.70	0.15	0.85	0.15	0.49	0.48	5.1	300	200	201.1	198.9	161.8	2.2	29.0	39.3	4	3
								5.2	400	300	298.9	296.6	264.0	2.3	32.7	34.9	6	3
								5.3	500	400	399.7	396.9	361.4	2.8	37.4	38.3	5	3
								5.4	600	500	498.8	496.3	457.1	2.5	40.6	41.7	7	4
								5.5	700	600	600.6	598.3	555.8	2.3	43.1	44.8	8	3

FIG. 3

Soil properties of the sandy silt: (*A*) particle size distribution; (*B*) soil–water retention curve.

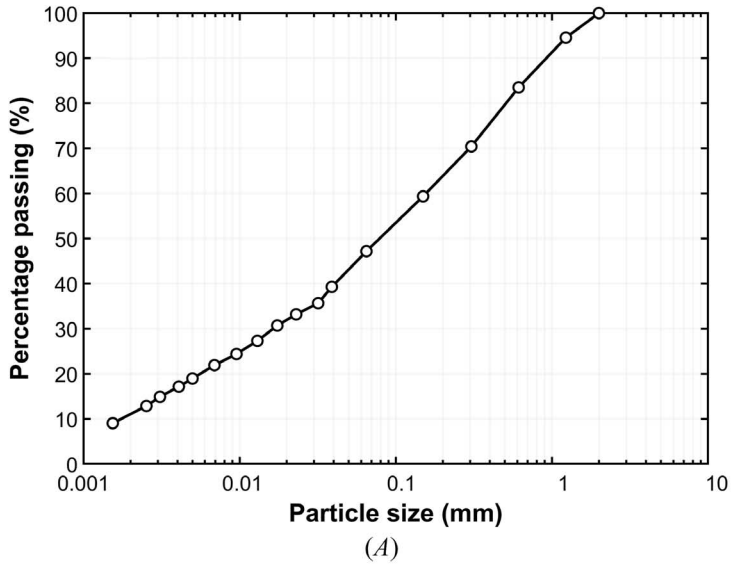

(*A*)

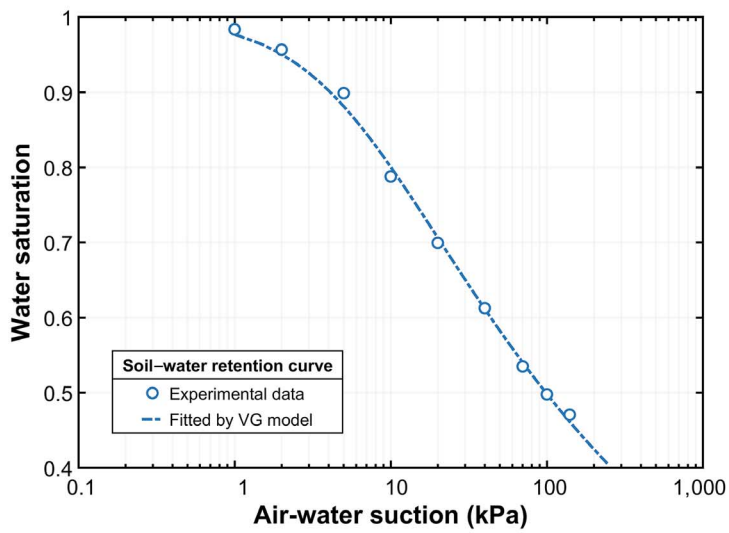

(*B*)

the oil and water retention curves of oil-contaminated soil. Additional geotechnical properties of the tested soils are provided in Table 3.

Although the hydro-mechanical behavior of oil-contaminated soils is likely influenced by the type of oil, including factors such as volatility, viscosity, and dielectric constant, it is preferable to use pure and stable oil during the verification stage of this apparatus. The oil used in this study is silicone oil, a nontoxic, pure, and stable material that has been used in previous studies for nonaqueous material testing (e.g., the oil infiltration test by Soga et al. 2003 and the nonequilibrium capillarity effects test by Goel and O'Carroll 2011). Silicone oil has similar dielectric constants and wettability to common oil contaminants such as petroleum hydrocarbons and motor oil, making it a useful choice for basic research. To minimize the test duration, this study selected the lowest viscosity silicone oil (XIAMETE PMX-200 Silicone Fluid). The properties of this silicone oil are presented in Table 4.

TABLE 3
Properties of tested soils

Parameter	Clean Sand	Sandy Silt (CDG)
Specific gravity	2.68	2.59
Liquid limit (%)		32
Plastic limit (%)		21
Plasticity index (%)		11
Maximum dry density (g/cm^3)	1.76	1.84
Optimum water content (%)		13.4
Particle size (mm)	0.25–0.5	0.001–2
Median particle size D_{50} (mm)	0.375	0.085
Sand content (2~0.063 mm)	100	50.8
Silt content (0.063~0.002 mm)	0	35.1
Clay content (≤0.002 mm)	0	14.1
Unified soil classification (ASTM D2487, 2011)	SP, poorly graded sand	ML, silt
van Genuchten model parameter: α (m^{-1}); van Genuchten model parameter: m		1.876; 0.189

TABLE 4
Properties of the silicone oil

Properties	Value
Product name	XIAMETE PMX-200 Silicone Fluid
Composition	Dimethicone
Specific gravity at 25°C	0.913
Kinematic viscosity at 25°C	5.0 cSt
Surface tension at 25°C	19.7 dynes/cm
Solubility parameter	7.1

Note: 5.0 cSt = 5.0 × 10^{-6} m^2/s; 19.7 dynes/cm = 19.7 × 10^{-3} N/m.

The sand specimen (20 mm in height and 100 mm in diameter) was prepared using the dynamic compaction method (Chapuis, Gill, and Baass 1989). The oven-dried sand was first mixed with 8.9 % water by mass and sealed for 48 hours. Then, the wet sand was compacted in a cylindrical container using five layers. The initial S_W of the compacted sand specimen was 0.40. The sandy silt specimens with the same size were prepared using static compaction. First, the silt was oven-dried and passed through a 2-mm sieve. Then, the dried silt was mixed with 10.2 % water by mass and sealed for 48 hours. After this time, the wet silt was compacted into an oedometer ring using five layers. The target dry density was 1.75 g/cm^3, resulting in a degree of compaction of 95 %. The initial S_W of all compacted silt specimens was 0.55.

To prepare the oil-contaminated specimens, calculated amounts of silicone oil were slowly dripped onto the top surface of specimens 1–4. Specimen 5 was watered and then contaminated with oil to reach a higher initial S_W of 0.70 while maintaining the same soil structure as the other silt specimens. Finally, the soil specimens were sealed and stored for 48 hours before testing for moisture equilibrium. In this study, the heterogeneous distribution of oil and water can be considered negligible for the 20-mm-high specimen. However, for higher height-to-diameter ratios (e.g., 2:1 in a triaxial test) in future studies, allowing more time for equilibrium is recommended.

The hydrophobic disk was saturated with silicone oil, whereas the hydrophilic disk was saturated with water prior to each test. The hydrophobic disk performed effectively during the tests conducted in this study. It is advisable to prevent its contact with water (except during the test) to extend its service life. One important issue related to these two disks is oil entrapment in the hydrophilic disk during and after the test, particularly when S_O exceeds 30 %. This entrapment can affect the accuracy of measurements during the test and the hydrophilic performance in subsequent tests. Therefore, long-term retention tests at high S_O should be avoided.

Results and Discussion

SUCTION CHANGES WITH INCREASING AIR PRESSURE AT CONSTANT OIL AND WATER CONTENT

The results of fluid pressure and suction measurements using the axis-translation technique are shown in figures 4–8 and summarized in Table 2. The specimen volume was monitored by the change in water volume in the cell. The void ratio of sand specimens remained almost unchanged at 0.35, and the average void ratio of silt specimens slightly decreased from 0.49 to 0.48. Figure 4 shows the pressure data for specimen No. 1 (clean sand), where the net normal stress was kept at 100 kPa. The upper half of the figure illustrates the air, oil, and water pressures observed during the test. It is evident that after each step, with a 10-kPa increase in both air and cell pressures, the oil and water pressures also increased by 10 kPa. In the lower half of the figure, the three suction histories during the testing are presented. The sand specimen reached equilibrium in each pressure stage after an average of 1.0 hour. The average equilibrium air–oil and air–water suctions were found to be 0.5 kPa and 1.5 kPa, respectively. Furthermore, the suctions at all five stages were very similar. Additionally, the ratio between these two sections closely resembled the ratio of oil and water surface tensions (0.27). It is just the scaling law that was firstly suggested by Leverett (1941) for the extension of two-phase S–P relationships to three phases and was described in the widely used S–P model (Parker, Lenhard, and Kuppusamy 1987):

$$P_{cAO} = [S_T^{-1/m} - 1]^{1-m} \alpha^{-1} \beta_{AO}^{-1} \tag{1}$$

$$\beta_{AO} = \sigma_{AW} / \sigma_{AO} \tag{2}$$

where P_{cAO} is the air–oil suction, S_T is the degree of total saturation equal to the sum of S_O and S_W, α is the coefficient of air-entry value in the VG model, β_{AO} is the surface tension ratio between air–water and air–oil, σ_{AW} is the air–water surface tension, and σ_{AO} is the air–oil surface tension. This equation has been extensively tested

FIG. 4

Time response curves for fluid pressures and suctions measurements using the axis-translation technique: No. 1.

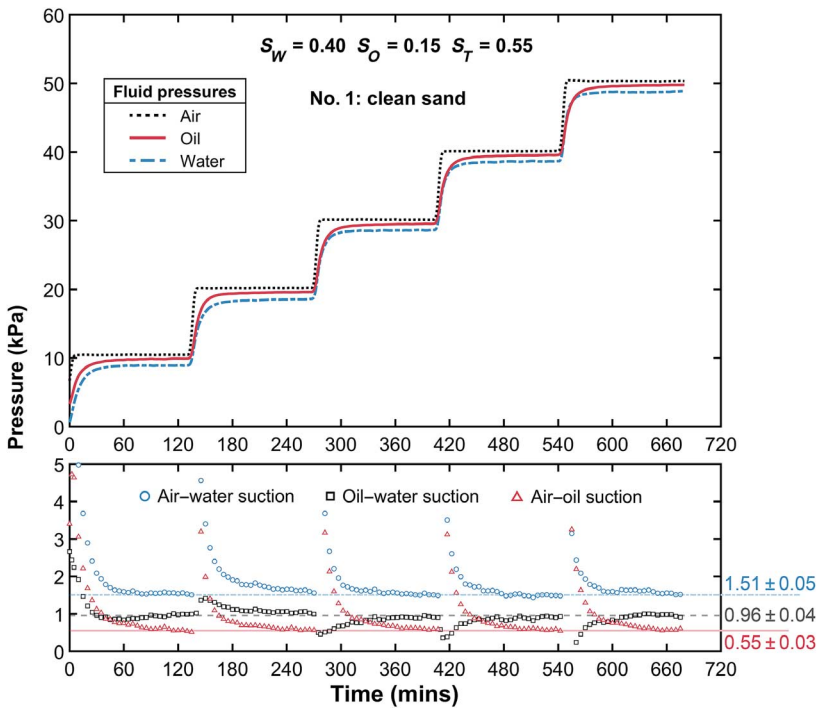

FIG. 5 Time response curves for fluid pressures and suctions measurements using the axis-translation technique: No. 2.

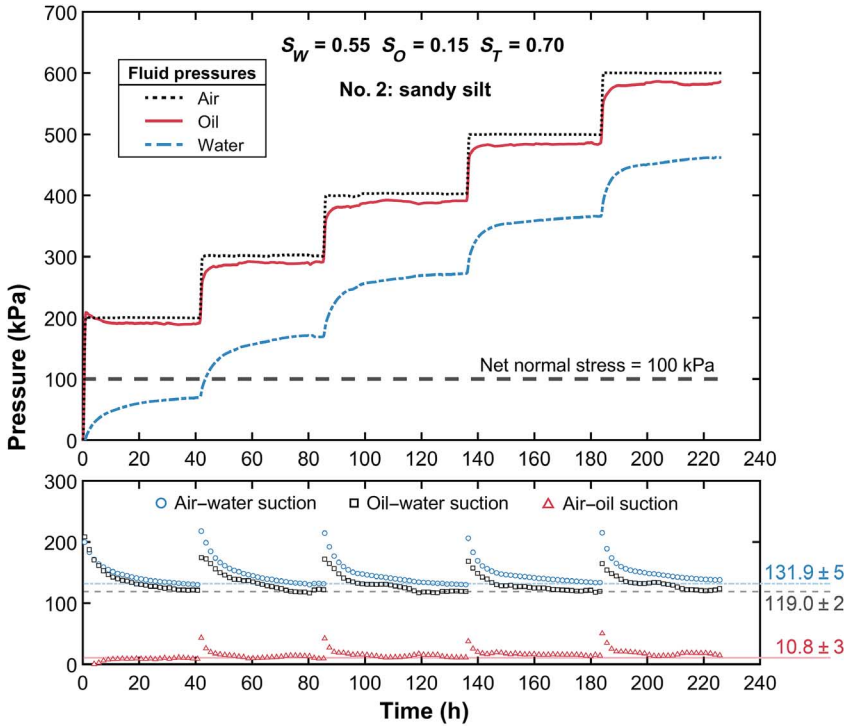

on the sand (Lenhard and Parker 1988; Busby, Lenhard, and Rolston 1995), and the result of this specimen is also consistent.

Figure 5 shows the pressure data for specimen No. 2 (sandy silt), where the pressure increment is 100 kPa at each pressure stage. The sequential increases of 100 kPa in cell, air, oil, and water pressures were also observed. The three suctions in the lower half of the figure showed a slower downward trend at each pressure stage, with the air–water suction trending toward 131.9 ± 5 kPa, the air–oil suction trending toward 10.8 ± 3 kPa, and the oil–water suction trending toward 10.8 ± 3 kPa.

The data from the other specimens showed similar trends in figures 5–8, albeit with different rates of change. A slight increase of air–oil and air–water suctions were observed in figure 8, possibly due to the slight decrease in S_O and S_W induced by air diffusion. The results in figures 4–8 suggest that all stress components and suctions had equal translations during the test. In other words, the increased air, water, and oil pressures and the increased normal stress were equal without any soil deformation during the test. Therefore, it can be concluded that the axis-translation technique is applicable for measuring three suctions in oil-contaminated soil, a solid–air–oil–water system.

EQUILIBRIUM TIME

The data shown in figures 4–8 indicate the significant difference of the equilibrium time between clean sand (1.0 hours) and sandy silt (4–20 hours). It is also worth noting that the incremental trends of oil and water pressures with time vary among the four silt specimens. Besides, the decremental trends of the three suctions also differed among the results. For instance, in specimen No. 4, the trend of the oil–water suction first decreased to the lowest value and then gradually increased, whereas the trends of the air–oil and air–water suctions flattened out at each stage. Further analysis of the equilibrium time in each test may provide more insights into these differences among silt specimens.

FIG. 6 Time response curves for fluid pressures and suctions measurements using the axis-translation technique: No. 3.

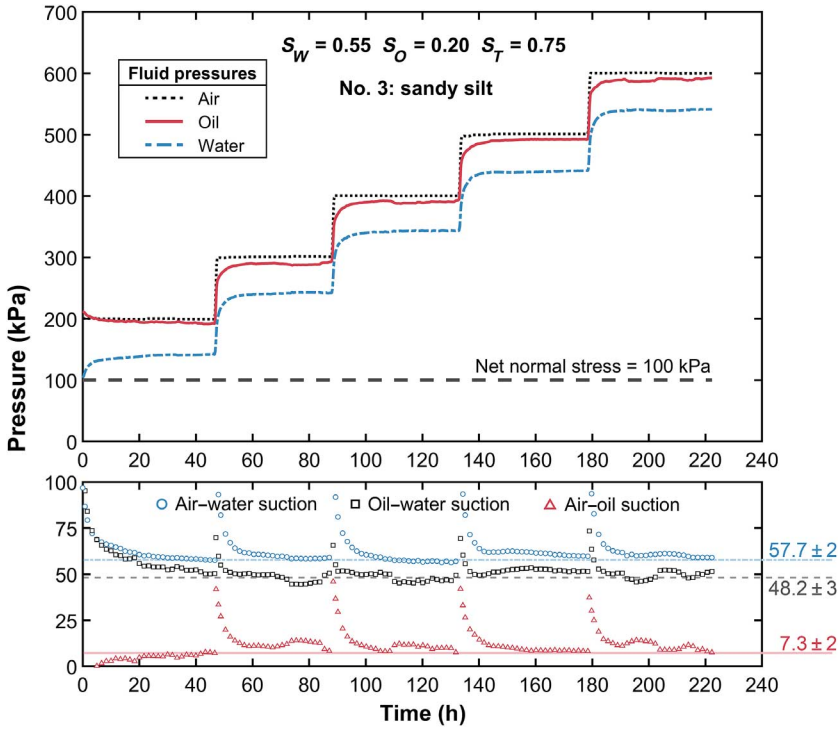

One challenge in using the axis-translation technique is the time required for the system to reach equilibrium, which can take several hours for a compacted specimen with a thickness of 20 mm (Vanapalli, Fredlund, and Pufahl 1999). To accurately determine the equilibrium time, it is necessary to establish a standard for pressure measurement. ASTM International provides a standard for suction less than 500 kPa (ASTM D6836-02, *Standard Test Methods for Determination of the Soil Water Characteristic Curve for Desorption Using a Hanging Column, Pressure Extractor, Chilled Mirror Hygrometer, and/or Centrifuge* (Superseded)), which states that the system is considered to be in equilibrium if no water drains for at least 24 hours. However, this standard is not applicable in the current study as there is no water volume change in the specimen and the boundary conditions are different. As a result, a different standard for determining equilibrium time in sandy silt is used in this study.

$$R_{n,i} = \left| \frac{\overline{P_i} - \overline{P_{i-1}}}{\Delta P_n} \right| \tag{3}$$

$$R_{n,i-1}, R_{n,i}, R_{n,i+1} < 5\% \tag{4}$$

where R is the rate of pressure changes per hour; $\overline{P_i}$ is the average pressure (oil or water) within the i-th hour; ΔP_n is the total pressure changes during the n-th stage; i is the elapsed time (hours) during this stage; and n is the stage number in each test, 1~5. The average pressure per hour is calculated to check whether an equilibrium condition has been reached. The rate of change in pressure is then determined by dividing the difference in average pressure between two consecutive hours by the total pressure change at that point. If this rate is less than 5 % for 3 consecutive hours, it is considered that the fluid pressure (either oil or water) has reached equilibrium. The middle hour of this period is recorded as the equilibrium time.

FIG. 7 Time response curves for fluid pressures and suctions measurements using the axis-translation technique: No. 4.

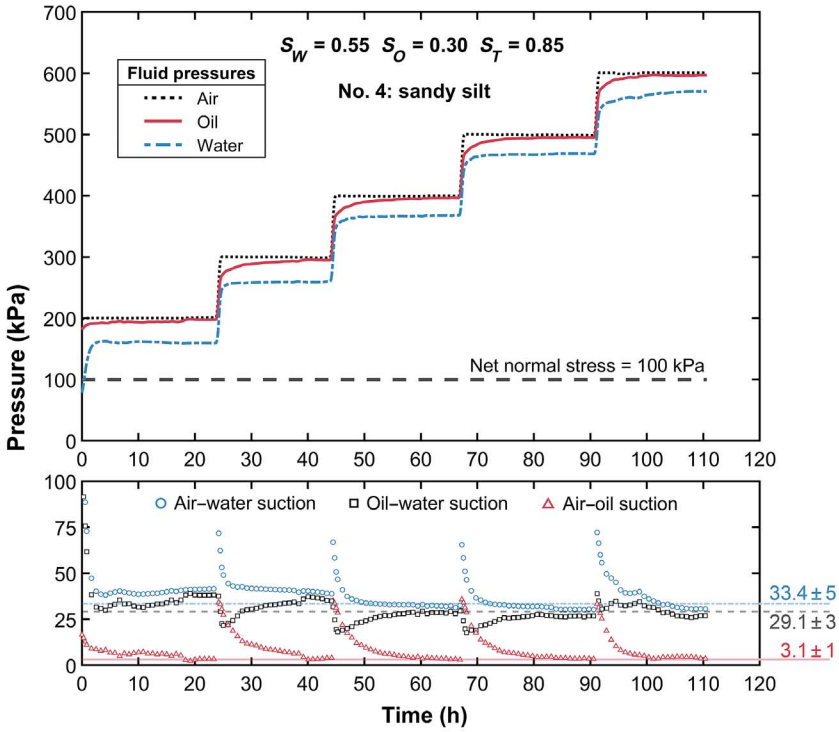

Figure 9 illustrates the relationship between fluid saturations and average equilibrium times for the silt specimens. When S_W increased from 0.55 to 0.70 (as shown in fig. 9A for specimens 2 and 5, with S_O kept at 0.15), the average equilibrium times of oil and water pressures were observed to decrease from 8.4 to 6.0 hours and 14.2 to 3.2 hours, respectively. This observation is consistent with the results reported by Cecchin et al. (2016) that the increase in soil moisture reduces the retention process of contaminants. When S_O increased from 0.15 to 0.30 (as shown in fig. 9B for specimens Nos. 2∼4, with S_W kept at 0.55, the average equilibrium time of water pressures also decreased significantly from 14.2 to 5.2 hours. However, the equilibrium time of oil had a slight increase from 8.4 to 9.8 hours. These results indicate that both increasing S_W and S_O can reduce the average equilibrium time of water pressure. Previous research had indicated that water permeability plays a dominant role influencing equilibrium time among the factors (such as soil type, specimen size and permeability, and pore size of the ceramic disk) (Vanapalli, Fredlund, and Pufahl 1999). The water permeability equation for unsaturated soil proposed by Mualem (1976) may be used to explain the different equilibrium times among these specimens.

$$k_W = K_{SW} \cdot S_W^{1/2}\left[1 - \left(1 - S_W^{1/m}\right)^m\right]^2 \tag{5}$$

where k_W is the permeability of water, K_{SW} is the saturated permeability of water, and m is the coefficient in the VG model. The K_{SW} of all sandy silt specimens is assumed to be the same because of the identical initial soil structure and constant net stress. The k_W has an exponential increase with increasing S_W. The equilibrium time is negatively correlated with water permeability, which is consistent with the results shown in figure 9A. However, it is worth noting that the measured equilibrium time of water also decreased as S_O increased, which cannot be explained solely by the permeability theory (water permeability is not influenced by S_O in theory). One potential reason could be the difference in surface tension between the air–water and oil–water interfaces. Air and oil are

FIG. 8 Time response curves for fluid pressures and suctions measurements using the axis-translation technique: No. 5.

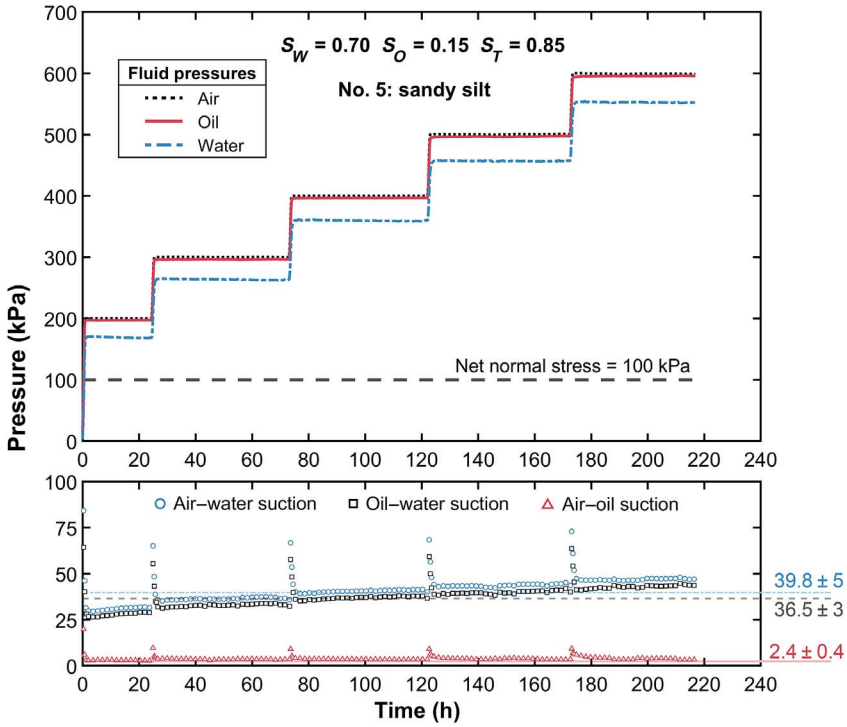

both nonwetting phases on the water surface, but oil is more wetting than air. As S_O increases, the average surface tension of the water with respect to these nonwetting phases decreases, which can facilitate more rapid equilibrium or redistribution of water. This difference in surface tension may explain the decrease in water equilibrium time as S_O increases.

For the permeability of oil, the equation goes with the following (Parker, Lenhard, and Kuppusamy 1987):

$$k_O = K_{SO} \cdot S_O^{1/2}[(1 - S_W^{1/m})^m - (1 - S_T^{1/m})^m]^2 \quad (6)$$

where k_O is the permeability of oil, and K_{SO} is the saturated permeability of oil. According to this equation, k_O has an exponential increase with increasing S_W and S_O (Yu, Zhou, and Mu 2022), and S_W is a key factor in this process. This may help to explain the experimental finding that the measured oil equilibrium time decreased as S_W increased. Although the average equilibrium time of oil did show an increasing trend with increasing S_O, the increase was relatively small, with the time remaining within the range of 8 to 10 hours. It may be because the process of redistributing the increased S_O takes more time. In general, the initial saturation conditions affect the equilibrium time of water and oil, resulting in different convergence rates of the three suctions (figs. 5–8).

S-P RELATIONSHIP

Figure 10 shows the S-P relationship between equilibrium suctions and S_T. The average air–oil suction for oil-contaminated soil should be compared closely with equation (1). The trend shown in figure 10*A* is consistent with the theoretical prediction by the constitutive equation stating that the air–oil suction decreases with increasing S_T. This indicates that the model is still applicable in sandy silt. It is worth noting that the error range in figure 10*A* is acceptable because of the low air–oil suction (less than 20 kPa) and the fluctuation of the air source (which can cause an error of ±1 kPa).

FIG. 9 Fluid saturations versus average equilibrium time of pressures: (*A*) water saturation varied from 0.55 to 0.70 when oil saturation = 0.15; (*B*) oil saturation varied from 0.15 to 0.30 when water saturation = 0.55.

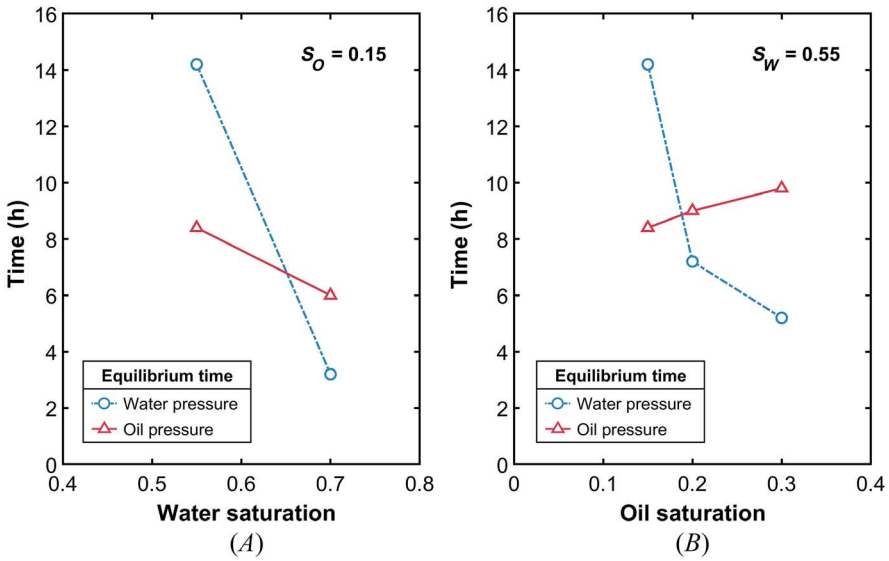

For oil–water suction, the constitutive equation (Parker, Lenhard, and Kuppusamy 1987) goes with the following:

$$P_{cOW} = [S_W^{-1/m} - 1]^{1-m} \alpha^{-1} \beta_{OW}^{-1} \tag{7}$$

$$\beta_{OW} = \sigma_{AW} / \sigma_{OW} \tag{8}$$

where P_{cOW} is the oil–water suction, β_{OW} is the surface tension ratio between air–water and oil–water, and σ_{OW} is the oil–water surface tension. According to existing models, the oil–water suction should only depend on the specimen's S_W. **Figure 10*B*** shows the S–P relationship between S_W and oil–water suction. The results indicate that when S_W is held constant at 0.55, the average oil–water suction decreases from 119.0 to 36.6 kPa as S_O increases from 0.15 to 0.30. This does not align with the prediction of equation (7), which is represented by the dashed line. The deviation between the experimental data and the constitutive model for oil–water suction suggests that the model may need to be revised. One of the potential reasons may be the oil entrapment process when the soil specimen has a higher clay content than sand. Previous research on unsaturated soil has shown that the clay content can significantly impact the soil particle skeleton at different water contents and following moisture distribution (Delage et al. 1996). The formation of the soil could affect the volume of oil that is trapped and residual, as well as the surface area between different fluid pairs in the interphase (Sookhak Lari et al. 2019). The complexity of the actual oil entrapment in this CDG may result in a deviation between the experimental results and the prediction, which is different from what is described by equation (7).

Summary and Conclusions

A triaxial testing apparatus has been developed for testing the hydro-mechanical behavior of multiphase oil-contaminated unsaturated soil. Hydrophobic and hydrophilic ceramic disks are used to measure the pressures of water and oil independently. This apparatus is capable of conducting retention, isotropic compression, and triaxial shear tests, as well as measuring soil deformation during the test under different stress conditions. The

FIG. 10

Total saturation versus equilibrium suctions: (*A*) air–oil suction; (*B*) oil–water suction.

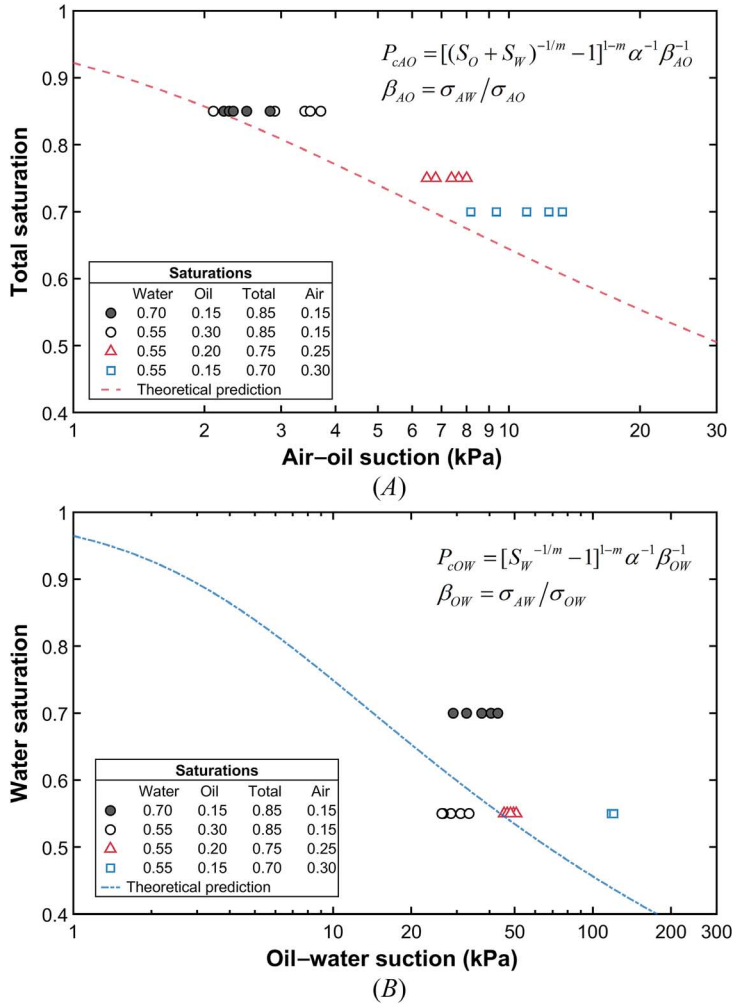

apparatus utilizes the hanging column or axis-translation technique to control the suction levels, allowing for an increased range of available suction up to 600 kPa. This makes the apparatus suitable for a wider range of soil types, including silt and clay. A customized nitrile rubber membrane is adopted to substitute the conventional latex membrane to avoid oil corrosion. In addition, an LVDT is used to measure the sample volume during the testing.

One sand specimen and four CDG specimens with different initial saturations were tested to evaluate the feasibility of the axis-translation technique in this apparatus. During the experiments, a general downward trend in the air–oil, air–water, and oil–water suctions were observed after increases in air pressure, with terminal pressures remaining within a small range (around ±0.05 kPa in sand and ±5 kPa in CDG). This demonstrates the feasibility of using the axis-translation technique to control fluid suctions in the solid–air–oil–water system. The average equilibrium time of water and oil pressures was observed and linked to S_W and S_O.

In the model evaluation based on the test results on CDG, the air–oil suction data showed a good agreement with the prediction of the existing *S*–*P* model. However, the oil–water suction results did not align with the model prediction, indicating that the model may need to be revised for soils with a higher clay content than sand. To further investigate the hydro-mechanical behavior of oil-contaminated soil, microstructure experiments should

be further conducted to check the oil entrapment in silt/clay, in addition to more tests such as isotropic compression and triaxial shear tests using the new apparatus.

ACKNOWLEDGMENTS

This work is supported by the Research Grants Council of the HKSAR (16204817). The authors also thank the Shenzhen Science and Technology Innovation Commission through grant 2022N040. This work was also supported by RISUD/PolyU under Grant 1-BBWS.

References

Abidoye, L. K. and D. B. Das. 2014. "Scale Dependent Dynamic Capillary Pressure Effect for Two-Phase Flow in Porous Media." *Advances in Water Resources* 74 (December): 212–230. https://doi.org/10.1016/j.advwatres.2014.09.009

Ahmadinezhad, A., F. Jafarzadeh, and H. Sadeghi. 2019. "Combination of Water Head Control and Axis Translation Techniques in New Unsaturated Cyclic Simple Shear Tests." *Soil Dynamics and Earthquake Engineering* 126 (November): 105818. https://doi.org/10.1016/j.soildyn.2019.105818

ASTM International. 2011. *Standard Practice for Classification of Soils for Engineering Purposes (Unified Soil Classification System)* (Superseded). ASTM D2487-11(2011). West Conshohocken, PA: ASTM International, approved May 1, 2011. https://doi.org/10.1520/D2487-11

ASTM International. 2008. *Standard Test Methods for Determination of the Soil Water Characteristic Curve for Desorption Using a Hanging Column, Pressure Extractor, Chilled Mirror Hygrometer, and/or Centrifuge* (Superseded). ASTM D6836-02(2008). West Conshohocken, PA: ASTM International, approved September 1, 2001. https://doi/org.10.1520/D6836-02R08E02

ASTM International. 2017. *Standard Test Method for Particle Size Distribution (Gradation) of Fine-Grained Soils Using the Sedimentation (Hydrometer Analysis).* ASTM D7928-17(2017). West Conshohocken, PA: ASTM International, approved May 1, 2021. https://www.doi.org/10.1520/D7928-21E01

Boumaiza, L., R. Chesnaux, J. Walter, R. J. Lenhard, S. M. Hassanizadeh, Z. Dokou, and M. Y. Alazaiza. 2022. "Predicting Vertical LNAPL Distribution in the Subsurface under the Fluctuating Water Table Effect." *Groundwater Monitoring & Remediation* 42, no. 2 (Spring): 47–58. https://doi.org/10.1111/gwmr.12497

Busby, R. D., R. J. Lenhard, and D. E. Rolston. 1995. "An Investigation of Saturation-Capillary Pressure Relations in Two-and Three-Fluid Systems for Several NAPLS in Different Porous Media." *Groundwater* 33, no. 4 (July): 570–578. https://doi.org/10.1111/j.1745-6584.1995.tb00312.x

Cassiani, G., A. Binley, A. Kemna, M. Wehrer, A. F. Orozco, R. Deiana, J. Boaga, et al. 2014. "Noninvasive Characterization of the Trecate (Italy) Crude-Oil Contaminated Site: Links between Contamination and Geophysical Signals." *Environmental Science and Pollution Research International* 21, no. 15 (August): 8914–8931. https://doi.org/10.1007/s11356-014-2494-7

Cecchin, I., C. Reginatto, A. Thomé, L. M. Colla, and K. R. Reddy. 2016. "Influence of Physicochemical Factors on Biodiesel Retention in Clayey Residual Soil." *Journal of Environmental Engineering* 142, no. 4 (April): 04015093. https://doi.org/10.1061/(ASCE)EE.1943-7870.0001060

Chapuis, R. P., D. E. Gill, and K. Baass. 1989. "Laboratory Permeability Tests on Sand: Influence of the Compaction Method on Anisotropy." *Canadian Geotechnical Journal* 26, no. 4 (November): 614–622. https://doi.org/10.1139/t89-074

Cui, Y., P. Delage, and P. Alzoghbi. 2003. "Retention and Transport of a Hydrocarbon in a Silt." *Géotechnique* 53, no. 1 (February): 83–91. https://doi.org/10.1680/geot.2003.53.1.83

Delage, P., M. Audiguier, Y.-J. Cui, and M. D. Howat. 1996. "Microstructure of a Compacted Silt." *Canadian Geotechnical Journal* 33, no. 1 (March): 150–158. https://doi.org/10.1139/t96-030

Essaid, H. I., B. A. Bekins, W. N. Herkelrath, and G. N. Delin. 2011. "Crude Oil at the Bemidji Site: 25 Years of Monitoring, Modeling, and Understanding." *Groundwater* 49, no. 5 (September/October): 706–726. https://doi.org/10.1111/j.1745-6584.2009.00654.x

Goel, G. and D. M. O'Carroll. 2011. "Experimental Investigation of Nonequilibrium Capillarity Effects: Fluid Viscosity Effects." *Water Resources Research* 47, no. 9 (September): W09507. https://doi.org/10.1029/2010WR009861

Lenhard, R. 1992. "Measurement and Modeling of Three-Phase Saturation-Pressure Hysteresis." *Journal of Contaminant Hydrology* 9, no. 3 (March): 243–269. https://doi.org/10.1016/0169-7722(92)90007-2

Lenhard, R. J. and J. C. Parker. 1988. "Experimental Validation of the Theory of Extending Two-Phase Saturation-Pressure Relations to Three-Fluid Phase Systems for Monotonic Drainage Paths." *Water Resources Research* 24, no. 3 (March): 373–380. https://doi.org/10.1029/WR024i003p00373

Lenhard, R. J., J. L. Rayner, and G. B. Davis. 2017. "A Practical Tool for Estimating Subsurface LNAPL Distributions and Transmissivity Using Current and Historical Fluid Levels in Groundwater Wells: Effects of Entrapped and Residual LNAPL." *Journal of Contaminant Hydrology* 205 (October): 1–11. https://doi.org/10.1016/j.jconhyd.2017.06.002

Lenhard, R. J., K. Sookhak Lari, J. L. Rayner, and G. B. Davis. 2018. "Evaluating an Analytical Model to Predict Subsurface LNAPL Distributions and Transmissivity from Current and Historic Fluid Levels in Groundwater Wells: Comparing

Results to Numerical Simulations." *Groundwater Monitoring & Remediation* 38, no. 1 (Winter): 75–84. https://doi.org/10.1111/gwmr.12254

Leverett, M. C. 1941. "Capillary Behavior in Porous Solids." *Transactions of the AIME* 142, no. 1 (December): 152–169, https://doi.org/10.2118/941152-G

Little, D. I. 2023. "Water Tables and Drainage Characteristics of Intertidal Sediments: Lessons for (and from) Oil Spill Response and Remediation." *Estuarine, Coastal and Shelf Science* 283 (April): 108245. https://doi.org/10.1016/j.ecss.2023.108245

Mualem, Y. 1976. "A New Model for Predicting the Hydraulic Conductivity of Unsaturated Porous Media." *Water Resources Research* 12, no. 3 (June): 513–522. https://doi.org/10.1029/WR012i003p00513

Nasr, A. M. 2009. "Experimental and Theoretical Studies for the Behavior of Strip Footing on Oil-Contaminated Sand." *Journal of Geotechnical and Geoenvironmental Engineering* 135, no. 12 (December): 1814–1822. https://doi.org/10.1061/(ASCE)GT.1943-5606.0000165

Nasr, A. M. 2013. "Uplift Behavior of Vertical Piles Embedded in Oil-Contaminated Sand." *Journal of Geotechnical and Geoenvironmental Engineering* 139, no. 1 (January): 162–174. https://doi.org/10.1061/(ASCE)GT.1943-5606.0000739

Ng, C. W. W., C. Zhou, and A. K. Leung. 2015. "Comparisons of Different Suction Control Techniques by Water Retention Curves: Theoretical and Experimental Studies." *Vadose Zone Journal* 14, no. 9 (September): 1–9. https://doi.org/10.2136/vzj2015.01.0006

Ossai, I. C., A. Ahmed, A. Hassan, and F. S. Hamid. 2020. "Remediation of Soil and Water Contaminated with Petroleum Hydrocarbon: A Review." *Environmental Technology & Innovation* 17 (February): 100526. https://doi.org/10.1016/j.eti.2019.100526

Parker, J. C., R. J. Lenhard, and T. Kuppusamy. 1987. "A Parametric Model for Constitutive Properties Governing Multiphase Flow in Porous Media." *Water Resources Research* 23, no. 4 (April): 618–624. https://doi.org/10.1029/WR023i004p00618

Sale, T., H. Hopkins, and A. Kirkman. 2018. *Managing Risk at LNAPL Sites—Frequently Asked Questions, Bulletin No. 18*. Washington, DC: American Petroleum Institute.

Soga, K., J. Kawabata, C. Kechavarzi, H. Coumoulos, and W. Waduge. 2003. "Centrifuge Modeling of Nonaqueous Phase Liquid Movement and Entrapment in Unsaturated Layered Soils." *Journal of Geotechnical and Geoenvironmental Engineering* 129, no. 2 (February): 173–182. https://doi.org/10.1061/(ASCE)1090-0241(2003)129:2(173)

Tomlinson, D. W., S. F. Thornton, A. O. Thomas, S. A. Leharne, and G. P. Wealthall. 2014. *An Illustrated Handbook of LNAPL Transport and Fate in the Subsurface*. London: Contaminated Land: Applications in Real Environment (CL:AIRE).

Sookhak Lari, K., G. B. Davis, J. L. Rayner, T. P. Bastow, and G. J. Puzon. 2019. "Natural Source Zone Depletion of LNAPL: A Critical Review Supporting Modelling Approaches." *Water Research* 157 (June): 630–646. https://doi.org/10.1016/j.watres.2019.04.001

van Genuchten, M. Th. 1980. "A Closed-Form Equation for Predicting the Hydraulic Conductivity of Unsaturated Soils." *Soil Science Society of America Journal* 44, no. 5 (September–October): 892–898. https://doi.org/10.2136/sssaj1980.03615995004400050002x

Vanapalli, S. K., D. G. Fredlund, and D. E. Pufahl. 1999. "The Influence of Soil Structure and Stress History on the Soil–Water Characteristics of a Compacted Till." *Géotechnique* 49, no. 2 (April): 143–159. https://doi.org/10.1680/geot.1999.49.2.143

Vanapalli, S. K., M. V. Nicotera, and R. S. Sharma. 2009. "Axis Translation and Negative Water Column Techniques for Suction Control." *Geotechnical and Geological Engineering* 26, no. 6 (December): 645–660. https://doi.org/10.1007/s10706-008-9206-3.

Wang, L., Y. Cheng, D. Lamb, and R. Naidu. 2020. "The Application of Rapid Handheld FTIR Petroleum Hydrocarbon-Contaminant Measurement with Transport Models for Site Assessment: A Case Study." *Geoderma* 361 (March): 114017. https://doi.org/10.1016/j.geoderma.2019.114017

Ye, B., J. Lu, and G. Ye. 2015. "Pre-shear Effect on Liquefaction Resistance of a Fujian Sand." *Soil Dynamics and Earthquake Engineering* 77 (October): 15–23. https://doi.org/10.1016/j.soildyn.2015.04.018

Yu, J. R., C. Zhou, and Q. Y. Mu. 2022. "Numerical Investigation on Light Non–aqueous Phase Liquid Flow in the Vadose Zone Considering Porosity Effects on Soil Hydraulic Properties." *Vadose Zone Journal* 21, no. 5 (September/October): e20211. https://doi.org/10.1002/vzj2.20211